Photon path length distributions inferred from rotating shadowband spectrometer measurements at the Atmospheric Radiation Measurements Program Southern Great Plains site

Qilong Min
Atmospheric Sciences Research Center, State University of New York, Albany, New York, USA

Eugene E. Clothiaux
Department of Meteorology, Pennsylvania State University, University Park, Pennsylvania, USA

Received 19 September 2002; revised 13 February 2003; accepted 13 March 2003; published 9 August 2003.

[1] An algorithm for retrieving the first two moments of the photon path length probability density function for both the oxygen A-band and the 0.820 μm water vapor band from measurements of the second generation Rotating Shadowband Spectrometer (RSS) is developed and applied to data from the Atmospheric Radiation Measurements (ARM) Program Southern Great Plains (SGP) site. In the algorithm, solar direct-beam measurements are used to characterize the instrument response function in pixel (i.e., wavelength) space. By using nonlinear least squares regression with a two-parameter gamma function constraint, the mean and variance of the photon path length probability density function for cloudy skies are subsequently retrieved from spectral measurements in both bands. Two case studies illustrate that the variance of the photon path length probability density function is more sensitive than the mean of the probability density function to vertical cloud structure. Interestingly, the first two moments of the photon path length probability density function appear to exhibit sufficient sensitivity to detect cirrus that the ARM SGP millimeter-wave cloud radar failed to detect. Photon path length probability density functions from both the oxygen A-band and 0.820 μm water vapor band provide additional insights into radiative transfer through a variety of cloudy conditions, improving our understanding of water vapor absorption of solar radiation in these conditions. *INDEX TERMS:* 0320 Atmospheric Composition and Structure: Cloud physics and chemistry; 0360 Atmospheric Composition and Structure: Transmission and scattering of radiation; 1640 Global Change: Remote sensing; *KEYWORDS:* cloud, aerosol, radiative transfer, remote sensing, path length, oxygen A-band

Citation: Min, Q., and E. E. Clothiaux, Photon path length distributions inferred from rotating shadowband spectrometer measurements at the Atmospheric Radiation Measurements Program Southern Great Plains site, *J. Geophys. Res.*, *108*(D15), 4465, doi:10.1029/2002JD002963, 2003.

1. Introduction

[2] Our understanding of, and ability to predict, climate change is currently limited by incomplete knowledge of climate forcing mechanisms and the response of the climate system to these mechanisms [*Intergovernmental Panel on Climate Change* (*IPCC*), 2001]. Aerosols, clouds, and water vapor are important components in a variety of climate forcing mechanisms, as they play key roles in the atmospheric energy balance and the hydrological cycle. Atmospheric increases in water vapor, an important "greenhouse gas" and the dominant gaseous absorber in the shortwave region of the electromagnetic spectrum, owing to doubled CO_2 can potentially lead to feedbacks that are larger than those due to the initial increase in CO_2 [*IPCC*, 1990]. Cloud horizontal inhomogeneity directly influences solar radiation transport both horizontally between clouds and vertically between the surface and space [*Cahalan et al.*, 1994]. The vertical structure of clouds determines the amount of infrared radiation that is absorbed and emitted by clouds and exchanged between clouds and the surface [*Stephens*, 1999]. Ultimately, advances in climate modeling will require proper treatment of radiation transfer in inhomogeneous cloud systems with their attendant water vapor fields.

[3] The application of fully developed techniques for retrieving photon path length distributions across a wide range of atmospheric conditions holds tremendous potential for advancing three-dimensional cloud and radiative transfer studies, as these distributions are intimately linked to the properties of a multiple scattering medium [*Stephens and Heidinger*, 2000; *Heidinger and Stephens*, 2000]. Because oxygen is a well-mixed gas in the atmosphere, the pressure dependence of oxygen A-band absorption line parameters at

0148-0227/03/2002JD002963$09.00

approximately 0.763 μm provides a vehicle for retrieving photon path length distributions from spectrometry of the oxygen A-band. The principle of equivalence subsequently allows conclusions to be drawn about the radiative properties of the atmosphere at wavelengths near the oxygen A-band from the oxygen A-band photon path length distributions [*van de Hulst*, 1980; *Partain et al.*, 2000] because the scattering properties of clouds and aerosols vary slowly and predictably with wavelength in this spectral region.

[4] To date the primary use of oxygen A-band remote sensing has been the retrieval of surface pressure and cloud top heights from satellite measurements [*Fischer and Grassl*, 1991; *Fischer et al.*, 1991; *O'Brian and Mitchell*, 1992] and the retrieval of path length distributions from ground- and airborne-based measurements [*Grechko et al.*, 1973; *Harrison and Min*, 1997; *Pfeilsticker et al.*, 1998; *Veitel et al.*, 1998; *Min and Harrison*, 1999; *Portmann et al.*, 2001; *Min et al.*, 2001]. All of these results have depended on limited information, effectively little more than one eigenvector from oxygen A-band spectroscopy measurements, though differently used.

[5] In a series of studies we have evolved a retrieval of atmospheric pressure- and temperature-weighted mean photon path length using the moderate resolution Rotating Shadowband Spectrometer (mrRSS) [*Min and Harrison*, 1999; *Min et al.*, 2001]. Here we extend our previous work by employing advanced Rotating Shadowband Spectrometer (aRSS) measurements in our retrieval that have triple the resolution of those from the mrRSS together with much better wavelength stability. As we demonstrate, use of the aRSS allows retrieval of the variance of the photon path length distribution in addition to the mean of the distribution. Furthermore, simultaneous measurements by the aRSS in the water vapor absorption band at approximately 0.820 μm provide information on how scattering processes, particularly in layered or complex cloud scenes, are influencing water vapor absorption. These retrieved quantities from aRSS measurements provide insight into the distribution of water vapor absorption of solar radiation, as modulated by clouds, and serve as a data set against which numerical weather prediction and global climate model cloud parameterizations can be tested for fidelity to real atmospheres.

2. Retrieval of Oxygen A-Band and Water Vapor Band Photon Path Length Distributions

[6] When radiation arrives to a sensor via multiple paths, the Bouguer-Lambert-Beer law can be written as

$$\frac{I(\lambda)}{I_0(\lambda)} = \int_0^\infty e^{-\chi(\lambda)l} P(l)dl,$$

where $I(\lambda)$ is the atmospheric irradiance with wavelength λ at the sensor, $I_0(\lambda)$ is the irradiance at the sensor in the absence of atmospheric absorption processes, $\chi(\lambda)$ is the absorption cross section (in m^2/g) of the relevant absorber, and l is the absorber amount (in g/m^2) along one of the possible photon trajectories. The probability density function (PDF) $P(l)$ expresses the probability that photons have traversed through l amount of absorber in the multiple-path case. Note that in the above equation both $\chi(\lambda)$ and l are for a homogeneous layer.

[7] The retrieval developed by *Min and Harrison* [1999] and *Min et al.* [2001] starts by recasting the above equation into integrated quantities across the depth of the atmosphere. Defining $\tau(\lambda)$ as the vertical absorption optical depth of the absorber of interest, they write the above equation in the form

$$\frac{I(\lambda)}{I_0(\lambda)} = \int_0^\infty e^{-\tau(\lambda)L} P(L)dL,$$

where

$$\tau(\lambda) = (p/p_0)^2 \tau_s(\lambda)$$

is the absorption optical depth for molecular oxygen away from line centers, where current instruments have sufficient accuracy for useful measurements, as a function of surface pressure p (p_0 is surface pressure for the standard atmosphere and $\tau_s(\lambda)$ is the absorption optical depth of molecular oxygen in the standard atmosphere) and

$$\tau(\lambda) = \tau(\lambda; C_{wvp})$$

is the absorption optical depth due to water vapor molecules given the column water vapor path (C_{wvp}) retrieved from microwave radiometer measurements. In this notation L is dimensionless and represents photon path lengths in increments of the vertical absorption optical depth $\tau(\lambda)$ traversed by photons as they travel through the atmosphere to the surface. Therefore the smallest value of L is one.

[8] The photon path length PDF $P(L)$ can be obtained from resolved absorption line measurements by a constrained inverse Laplace transform. The retrieval is sensitive to errors in the slit function and improves with higher resolution measurements that have reduced stray light. A critical issue in the retrieval is that each spectral irradiance measurement (i.e., pixel response) represents an integral over a wavelength region corresponding to the slit function of the pixel, which can be transformed into an integral over a distribution of the absorption optical depth $\tau(\lambda)$. The inversion kernel must contain accurate transmissions versus path length data for each of these integrals. The inversion is intractable if attempted by a "brute force" scheme of measuring the instrument slit functions and pixel responses directly in the laboratory and using them in conjunction with high-resolution solar spectral measurements and laboratory-measured O_2 and H_2O absorption spectra in an attempt to compute relevant transmissions. None of these measurements are sufficiently accurate or congruent to allow the necessary accuracies in the needed transmission kernels. To avoid these problems we have developed a new approach using the mrRSS and aRSS to infer photon path length distributions by obtaining empirical calibration coefficients from solar direct-beam observations.

[9] The aRSS is a CCD-array spectrograph coupled to an irradiance fore-optic described by *Harrison et al.* [1999]. It uses an automated shadow-banding technique to provide spectrally resolved solar direct-normal, diffuse-horizontal and total-horizontal irradiances, where the pass-

bands and pixel responses are guaranteed to be identical for the separated spectral irradiance components. For our purposes measurements of the solar direct beam under clear skies allow accurate calibration of the mean photon path length retrieval from oxygen A-band spectroscopy. Once calibrated, the retrieval can be applied to cloudy sky cases.

[10] For a measurement I_p at any particular pixel, corresponding to some spectral wavelength λ, we have

$$\frac{I_p}{I_{p,0}} = \int_0^\infty S_p(\tau) \int_0^\infty P(L) e^{-\tau L} dL \; d\tau,$$

where $S_p(\tau)$ is the slit function transformed from a function of wavelength λ to a function of absorption optical depth τ and $I_{p,0}$ is the irradiance measurement without atmospheric absorption at pixel p obtained from interpolation of the pixel irradiances at both ends of the absorption band. (Note that variations of aerosol and cloud optical properties across the absorption band are extremely small.) For the direct beam $P(L) = \delta(L - L_{db})$, where L_{db} is the solar zenith angle-dependent direct-beam path length from the top of atmosphere to the sensor. As discussed in the work of *Min and Harrison* [1999], measurements at each pixel result from the convolution of irradiances across the absorption band, including contributions from both weak and strong absorption lines. Hence they adopted the band model concept to characterize each pixel response, writing the transmittance as a simple polynomial function times an exponential function. Therefore for the direct beam we have

$$\frac{I_p^{dir}}{I_{p,0}^{dir}} = \int_0^\infty S_p(\tau) \int_0^\infty \delta(L - L_{db}) e^{-\tau L} dL \; d\tau$$

$$= \int_0^\infty S_p(\tau) e^{-\tau L_{db}} d\tau \approx \sum_{i=0}^{2} a_{p,i} \left(l_{db} - l_{off}\right)^i e^{-\tau_{p,0} l_{db}},$$

where $I_{p,0}^{dir}$ is the direct beam irradiance without atmospheric absorption at pixel p, l_{db} is the direct-beam path length in appropriate units, l_{off} is a path length offset in the same units as l_{db}, $a_{p,i}$ are the polynomial regression coefficients and $\tau_{p,0}$ is the exponential regression coefficient.

[11] In the regression fits the coefficient $\tau_{p,0}$ no longer varies with the surface pressure p and the column water vapor path C_{wvp}, as was the case for $\tau(\lambda)$. To compensate for this feature of the regression fits, we use l_{db} and l_{off} in the regression equations, instead of L and L_{db}, where l_{db} and l_{off} are dependent upon $(p/p_0)^2$ in the oxygen A-band and C_{wvp} in the 0.820 μm water vapor band. That is, l_{off} equals $(p/p_0)^2$ for the oxygen A-band retrievals and is dimensionless, while l_{off} equals C_{wvp} for the 0.820 μm water vapor band retrievals and has dimensions of g/m^2. The direct-beam paths l_{db} for oxygen and water vapor absorption are now $\mu\, l_{off}$, where μ is the number of air masses traversed by solar photons that reach the surface without any interactions within the atmosphere. Note that the coefficients $a_{p,i}$ and $\tau_{p,0}$ have units of $(\text{m}^2/\text{g})^i$ and m^2/g, respectively, for the water vapor band retrievals, while they are dimensionless for the oxygen A-band retrievals.

[12] In reality, the wavelength region corresponding to each individual pixel may drift as a result of temperature variations. However, we can monitor the wavelength shift s_w by registering the wavelength using oxygen A-band spectroscopy. Because of relatively small values for s_w, we can assume linear wavelength drifts in the transmittance model [*Min and Harrison*, 1999], obtaining

$$\frac{I_p^{dir}}{I_{p,0}^{dir}} = \int_0^\infty S_p(\tau) e^{-\tau L_{db}} d\tau$$

$$\approx \sum_{i=0}^{2} \left(a_{p,i} + b_{p,i} s_w\right) \left(l_{db} - l_{off}\right)^i e^{-\left(\tau_{p,0} + \tau_{p,1} s_w\right) l_{db}}.$$

For the diffuse irradiance we have

$$\frac{I_p^{dif}}{I_{p,0}^{dif}} = \int_0^\infty S_p(\tau) \int_0^\infty P(L) e^{-\tau L} dL \; d\tau$$

$$= \int_0^\infty P(L) \int_0^\infty S_p(\tau) e^{-\tau L} d\tau dL = \int_0^\infty P(L) \frac{I_p^{dir}}{I_{p,0}^{dir}} dL$$

$$\approx \sum_{i=0}^{2} \int_0^\infty P(l) \left(a_{p,i} + b_{p,i} s_w\right) \left(l - l_{off}\right)^i e^{-\left(\tau_{p,0} + \tau_{p,1} s_w\right) l} dl,$$

where $I_{p,0}^{dif}$ is the diffuse irradiance without atmospheric absorption and l, with the same units as l_{off}, represents path lengths for photons contributing to the diffuse irradiance. The quantity $I_{p,0}^{dif}$ is interpolated from irradiance measurements at the same pixels that we used for the direct beam and l can be written as Ll_{off}, where L is again a dimensionless real number greater than or equal to one. Assuming $P(l)$ to be a simple Gamma distribution and using the existence of the Laplace transform [*Harrison and Min*, 1997], we can simplify the above equation and obtain a reasonable constraint on the retrievals using the relation

$$\int_0^\infty x^\beta e^{-\alpha x} e^{-\tau x} dx = \frac{\Gamma(\beta + 1)}{(\tau + \alpha)^{\beta+1}}.$$

However, we must first modify this equation to allow a path length distribution with zero probability for lengths shorter than the one corresponding to the atmospheric depth. To do so we introduce $x = l - l_{off}$ and apply the general shift operator for the Laplace transform to obtain

$$\int_0^\infty \left(l - l_{off}\right)^\beta e^{-\alpha\left(l - l_{off}\right)} e^{-\tau l} dl = \frac{\Gamma(\beta + 1)}{(\tau + \alpha)^{\beta+1}} e^{-\tau l_{off}}.$$

With our assumption that $P(l) = \left(l - l_{off}\right)^\beta e^{-\alpha\left(l - l_{off}\right)}$, we now have

$$\frac{I_p^{dif}}{I_{p,0}^{dif}} = \sum_{i=0}^{2} \int_0^\infty \left(l - l_{off}\right)^\beta e^{-\alpha\left(l - l_{off}\right)} \left(a_{p,i} + b_{p,i} s_w\right)$$

$$\cdot \left(l - l_{off}\right)^i e^{-\left(\tau_{p,0} + \tau_{p,1} s_w\right) l} dl$$

$$= \sum_{i=0}^{2} \left(a_{p,i} + b_{p,i} s_w\right) \frac{\Gamma(\beta + i + 1)}{\left[\left(\tau_{p,0} + \tau_{p,1} s_w\right) + \alpha\right]^{\beta+i+1}} e^{-\left(\tau_{p,0} + \tau_{p,1} s_w\right) l_{off}},$$

where the coefficients $a_{p,i}$, $b_{p,i}$, $\tau_{p,0}$ and $\tau_{p,1}$ are constants obtained by fitting direct-beam measurements at each pixel as a function of solar air mass. We can now derive the

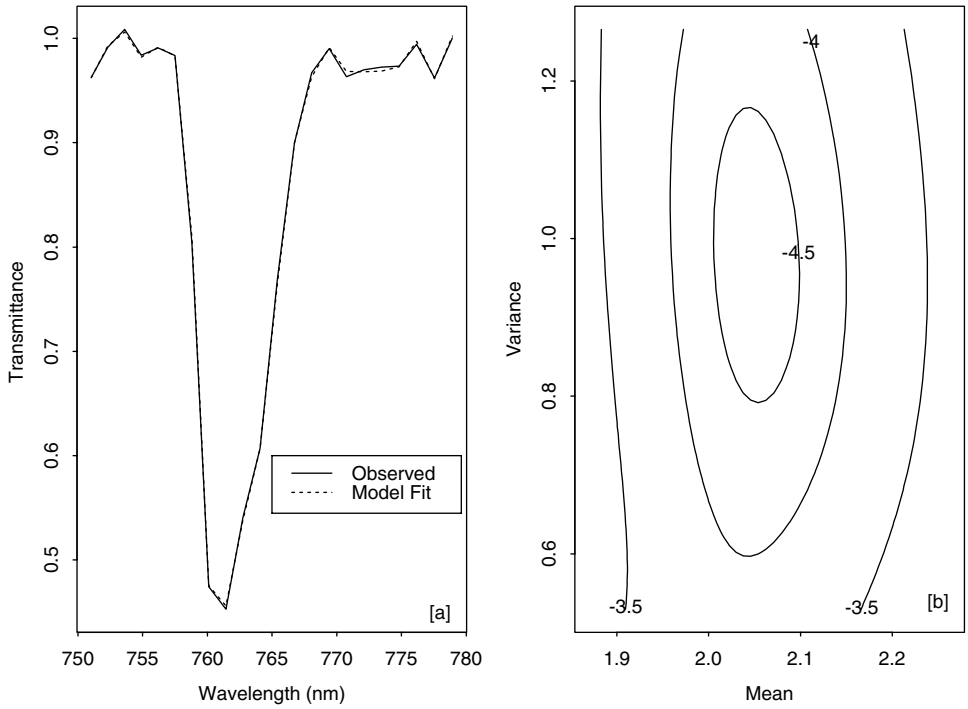

Figure 1. (a) Observed oxygen A-band spectrum together with model fit and (b) χ-squares of model fits under perturbations of the retrieved values for the mean and variance of the photon path length PDF. The χ-square contours in Figure 1b are given as logarithms to the base 10 of the actual χ-square values so that the minimum value in b) is -4.99.

photon path length distribution in both bands from the above analytical results by using nonlinear least-squares regression to estimate the coefficients β and α from spectral measurements.

[13] The photon path lengths retrieved above are in terms of l, or equivalently Ll_{off}, where L is a real number greater than or equal to one, l_{off} equals $(p/p_0)^2$ for the oxygen A-band and l_{off} equals C_{wvp} for the water vapor band. In order to compare results from the two bands, we first normalize the retrieved photon paths in the oxygen A-band by $(p/p_0)^2$ and those in the water vapor band by C_{wvp} to obtain photon path length distributions in terms of the dimensionless quantity L. Therefore in the results that follow the mean and variance are statistics of the photon path length probability density function $P(L)$. Consequently, they are dimensionless quantities and represent increments of $(p/p_0)^2$ for the oxygen A-band and C_{wvp} for the water vapor band.

3. Uncertainty Analysis and Information Content

[14] As discussed by *Min et al.* [2001], information on mean photon path length allows partial classification of cloud scenes, such as cloud layering and complex cloud structure with large photon path lengths and subvisual cirrus with small photon path lengths. *Min et al.* [2001] were limited by the resolution of the first generation mrRSS to retrieving only the mean photon path length. The second-generation aRSS has a resolution of 2.3 nm at the oxygen A-band and 0.820 μm water vapor bands, triple the resolution of the mrRSS, together with better out-of-band rejection compared to the mrRSS. These enhancements of the aRSS enable retrieval of the variance of the photon path length PDF in addition to the mean of the distribution, as we now show.

[15] To demonstrate that there is sufficient information content in aRSS measurements to retrieve the mean and variance of the photon path length PDF consider the cloudy sky measurements of $I_p^{dif}/I_{p,0}^{dif}$ illustrated in Figure 1a. Applying the retrieval to the measurements and computing the mean and variance of $P(L)$ with the retrieved α and β, we obtain 2.05 and 0.98 for the mean and variance, respectively, with a resulting χ-square of 1.03×10^{-5}. Note that the closeness of the regression fit to the data (Figure 1a) demonstrates that our transmittance model derived from solar direct-beam measurements for each pixel is valid for diffuse irradiance as a function of photon path length and properly implements wavelength registration corrections. Furthermore, we conclude that the two-parameter gamma function constraint on the photon path length PDF is a reasonable one. Introducing perturbations to the retrieved mean and variance of the photon path length PDF, we find that the χ-squares of the resulting fits are sensitive to changes in both parameters with gradients of steepest ascent along the parameter axes (Figure 1b). Hence aRSS measurements, with improved spectral resolution and out-of-band rejection, are sufficient to retrieve two independent pieces of information, i.e., the mean and variance of the photon path length PDF. Using the χ-square contours to quantify retrieval uncertainty that depends on measurement noise and wavelength stability, we conclude that the retrieved

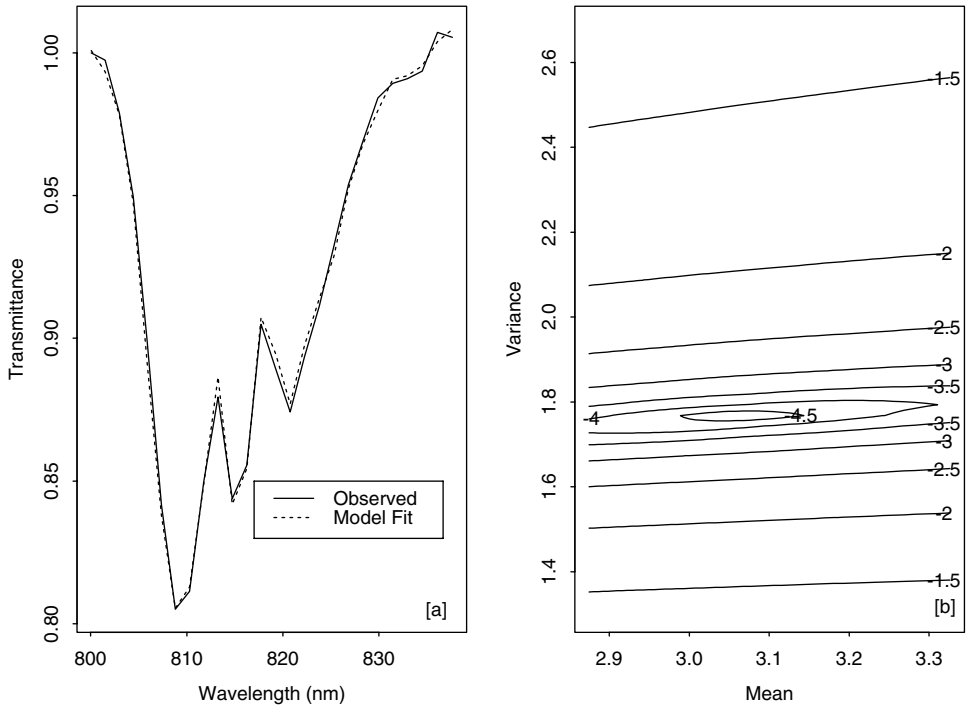

Figure 2. Same as Figure 1, but for the 0.820 μm water vapor band.

parameters have an uncertainty of about 5%. Note that we ensure the absolute accuracy of the retrieved quantities by using ratios of measurements in the retrieval. We find similar results for the 0.820 μm water vapor band (Figure 2).

4. Results

[16] To demonstrate the feasibility of the current retrieval we applied it to aRSS measurements during the ARESE II intensive observation period at the ARM SGP site. Using surface measurements of total horizontal transmittance at 0.415 μm either from a multifilter rotating shadowband radiometer or the aRSS, together with cloud liquid water path retrieved from a microwave radiometer, we simultaneously retrieved cloud optical depth and cloud drop effective radius through the use of a nonlinear least squares minimization in conjunction with an adjoint method of radiative transfer [*Min and Harrison*, 1996]. Retrieved optical depths less than 5 were subsequently replaced with values based on Beer's law using direct-beam extinction at 0.415 μm. We obtained cloud geometry and layer information from the millimeter-wave cloud radar and micro-pulse lidar using the algorithm of *Clothiaux et al.* [2000]. Both of these instruments are located within about 30 m of the radiation instruments at the ARM SGP site. We also used relative humidity profiles measured by a balloonborne sounding system to identify moist layers. Our analysis focuses on the two cloudy days of 3 and 29 March 2000.

4.1. Case 1: 3 March 2000

[17] On 3 March 2000, there were multiple cloud decks in the morning between 15:30 UTC and 18:00 UTC with a multiple tiered lower-level cloud deck in the afternoon between 19:00 UTC and 20:00 UTC and after 20:30 UTC (Figure 3a). For this case cloud optical depth varied from 5 to 78, while cloud-drop effective radius varied from 2.8 μm to 12.5 μm. The extremely small effective radius at 16:50 UTC may result from having thick ice clouds over lower-level water clouds because the ice water path, while having an impact on the total horizontal transmittance measurements by the multifilter rotating shadowband radiometer and aRSS, is not part of the cloud liquid water path retrieved by the microwave radiometer. Similar to the findings of *Min et al.* [2001], the mean photon path lengths are significantly enhanced owing to multiple scattering by multilayer clouds (Figure 3c). Moreover, the variances of the photon path length PDF in the oxygen A-band for the multilayer cloud periods are substantially enhanced over periods of single-layer cloud. Overall, these findings indicate that large values for the mean and variance of the photon path length PDF result from multilayer clouds. Both the mean and variance of the photon path length PDF in the water vapor band are well correlated with the corresponding oxygen A-band values. However, the ratios of the mean water vapor path lengths to mean oxygen A-band path lengths vary with time from 1.05 to 1.40 (Figure 3c) as the vertical profiles of cloud and water vapor change.

[18] Relative humidity profiles from the balloonborne sounding system for two periods, together with the retrieved photon path length PDFs in both bands for these two periods, are illustrated in Figure 4. The first sounding (Figure 4a) occurred during a single-layer cloud event when the cloud was located between 500 m and 1000 m. In this situation photons travel down to cloud top without much scattering and then are scattered within the cloud,

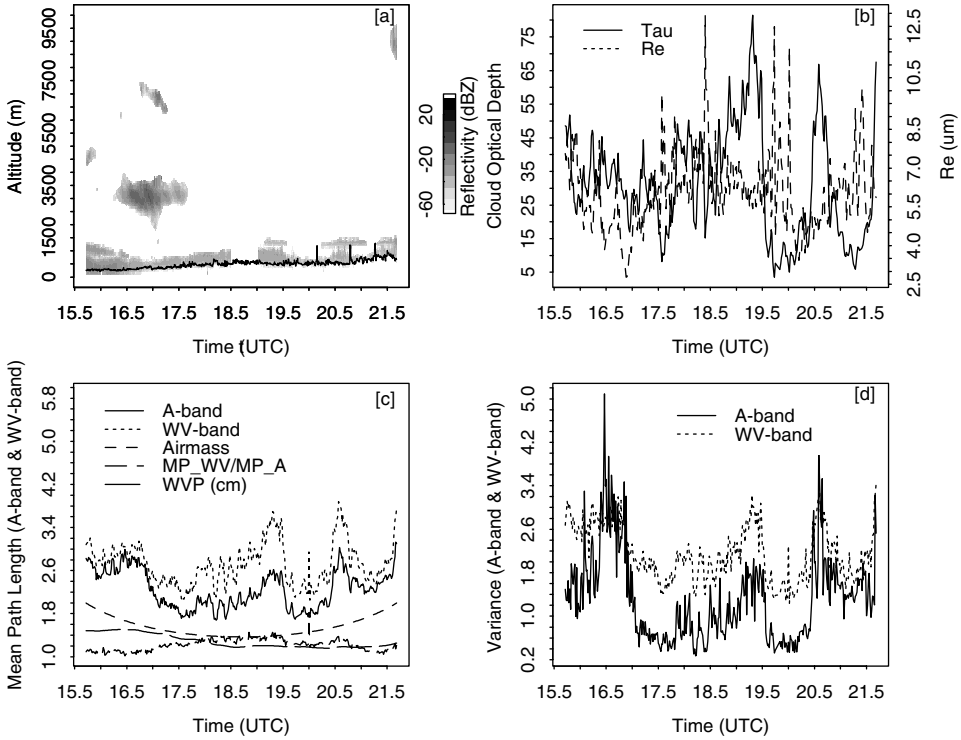

Figure 3. (a) Millimeter-wave cloud radar reflectivity, (b) cloud optical depth and effective radius, (c) mean and (d) variance of the photon path length PDFs in the oxygen A-band and water vapor band on 3 March 2000, at the ARM SGP site.

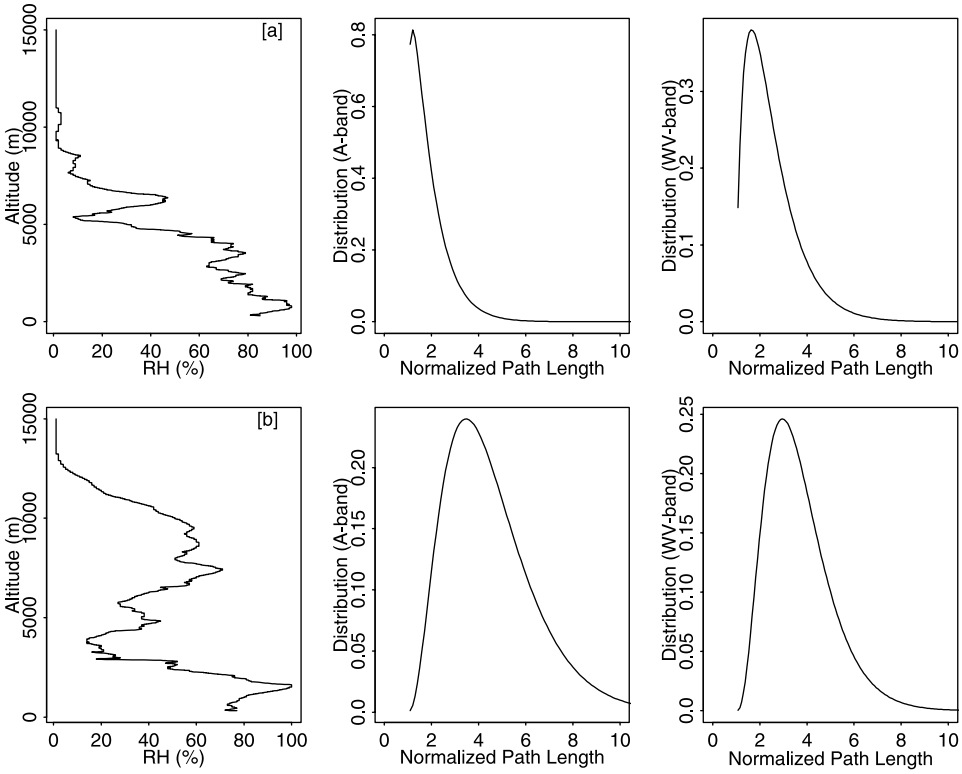

Figure 4. Balloonborne sounding system relative humidity profiles and coincident photon path length PDFs in the oxygen A-band and water vapor band on 3 March 2000 for (a) 18:02 UTC and (b) 23:45 UTC.

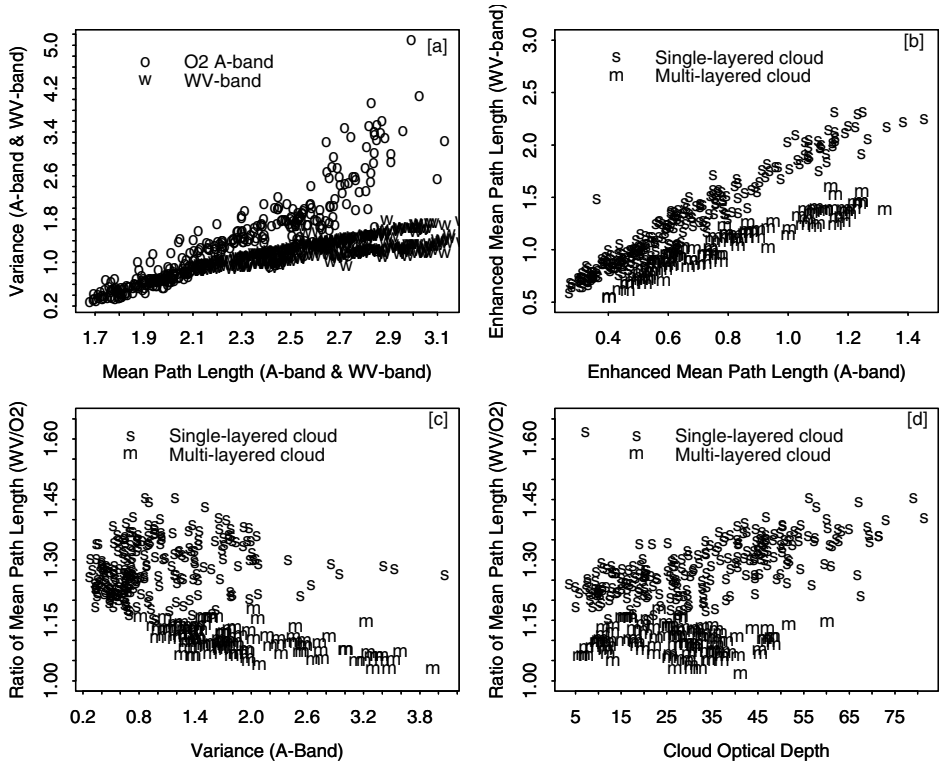

Figure 5. Joint statistics plots of (a) mean and variance of the photon path length PDFs for both bands, (b) enhanced mean path length in one band and the same quantity in the other band, (c) variance in the oxygen A-band path lengths and the ratio of mean water vapor band path length to mean oxygen A-band path length and (d) cloud optical depth and the ratio of mean water vapor band path length to mean oxygen A-band path length for 3 March 2000.

resulting in a relatively small spread in the photon path length PDFs with modes in the PDFs around two. For the double-layer cloud system that occurred during the second sounding (Figure 4b) the photon path length PDFs are broader with higher modal values. Photons are now bounced between the two cloud decks, in addition to being scattered within each cloud layer. While the photon path length PDFs for the water vapor band are similar to those for the oxygen A-band, differences in the photon path length PDFs for the single- and double-layer cloud decks are smaller for the water vapor band. For the two soundings most of the column water vapor is associated with the lowest cloud deck; hence multiple scatter of photons in the water vapor band above the lowest cloud deck does not increase total water vapor absorption, i.e., photon path length, that much.

[19] The current retrieval allows us to extend the joint statistics of mean photon path length and cloud optical depth presented by *Min and Harrison* [1999] and *Min et al.* [2001] for the oxygen A-band to include the water vapor band and the variance of the photon path length PDFs for both bands (Figure 5). As Figure 5a illustrates, the mean and variance of the photon path length PDFs are positively correlated with each other for both bands. The large scatter in Figure 5a for the oxygen A-band data is indicative of substantial changes in cloud geometry during the observation period. The water vapor data fall along two branches with quasi-linear correlations corresponding to variations in the vertical structure of water vapor and clouds illustrated by the data in Figures 3 and 4.

[20] A scatterplot of oxygen A-band versus water vapor band enhanced mean photon path length (i.e., total minus direct beam path length) for the case study period exhibits two branches with different slopes and intercepts (Figure 5b). Overall, there is a positive correlation between the enhanced mean photon path lengths between the two absorption bands, but the exact relationship between the two strongly depends on the vertical structure of water vapor and clouds. The branch with smaller slope and intercept corresponds to the periods before 17:50 UTC and after 21:30 UTC, when double-layer cloud systems were present with the upper layer clearly separated from the lower layer. As we described earlier, for this cloud situation photons bounce between the two cloud layers, substantially increasing the mean photon path length in the oxygen A-band while only marginally increasing the mean photon path length in the water vapor band because of the relative lack of water vapor between the two cloud layers. This point is also supported by the ratio of water vapor band to oxygen A-band mean photon path length, which decreases with increasing variance in the oxygen A-band photon path length PDFs (Figure 5c).

[21] The branch with the larger slope and intercept corresponds to the period between 17:50 UTC and 21:50 UTC

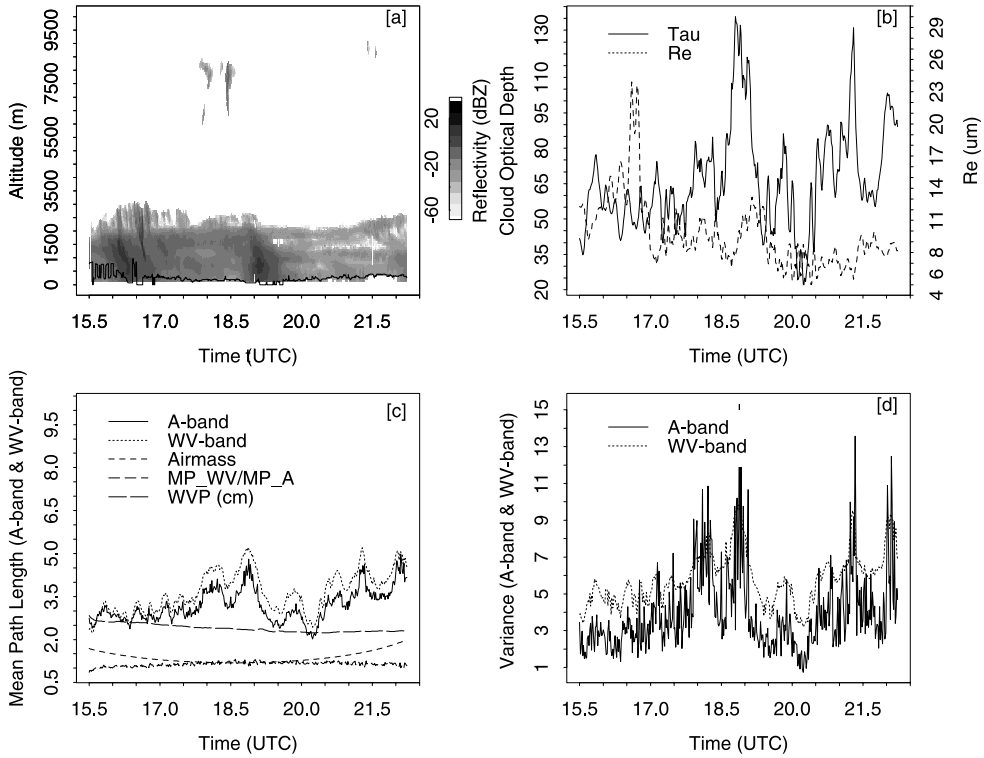

Figure 6. Same as Figure 3, but for 29 March 2000.

when most water vapor is located within and below the single-layer cloud deck. Note that periods of two-tiered clouds in the single-layer cloud deck (e.g., 19:00–19:50 UTC and 20:30–21:00 UTC) produce variances in the oxygen A-band photon path length PDF that are significantly larger than for the one-tiered cloud layer surrounding these periods. For the single-layer cloud deck the ratio of water vapor band to oxygen A-band mean photon path length is larger than for double-layer clouds and does not decrease with increasing variance in the oxygen A-band photon path length PDF (Figure 5c). These results indicate that within a single-layer cloud deck path length enhancement as a result of absorption by water vapor keeps pace with, or even exceeds, absorption in the oxygen A-band. In fact, for the single-layer cloud deck the ratio of mean photon path lengths actually increases with increasing cloud optical thickness (Figure 5d), which is what we would expect for enhanced scattering inside a cloud where the air is close to saturation. These results are a striking contrast to the results for the double-layer cloud system when the ratio showed no significant trend with cloud optical thickness, indicating that for the two-layer system accumulation of photon path length occurred between the two cloud layers.

4.2. Case 2: 29 March 2000

[22] The geometric and optical properties for the cloud system on 29 March 2000 are illustrated in Figure 6. The millimeter-wave cloud radar reflectivity time-height plot (Figure 6a) indicates that there was a thick low-level cloud layer with three brief periods of upper level cirrus during the case study period. Cloud optical depth varied from 20 to 130, while cloud-drop effective radius ranged from 5 μm to 12 μm except for a short period with values approaching 25 μm (Figure 6b). The large values of cloud-drop effective radius were due to overestimation of cloud-liquid water path from the microwave radiometer measurements because of water on the dome of the instrument. Note that the mean and variance of the photon path length PDF are significantly enhanced during the brief periods of cirrus around 18:20 UTC, 19:00 UTC and 21:30 UTC when scattering between cloud layers was important (Figures 6c and 6d). As for the first case study period, water vapor band and oxygen A-band mean photon path lengths were positively correlated. The ratio of water vapor band to oxygen A-band mean photon path length varied from 0.89 to 1.25 as the vertical profiles of water vapor changed under modulation by clouds.

[23] Interestingly, there is also a significant enhancement in the mean and variance of the photon path length PDF at 22:20 UTC, a period when the radar did not detect upper level cirrus. These results support the supposition that the oxygen A-band and water vapor band photon path length retrievals had sufficient sensitivity to detect cirrus that the radar failed to detect. While we found upper level clouds present in the morning and afternoon in GOES satellite imagery for this case study period, we could not conclusively establish the presence of upper level cloud near 22:20 UTC. Observations from the ARESE II aircraft team (R. Ellingson, personal communication, 2001) indicate that there was a haze layer over the low-level clouds during this period. Such a haze layer over low-level cloud would be difficult to detect with both surface-based active sensors and GOES satellite imagery. If such a layer was present for a brief period

around 22:20 UTC, this period would demonstrate the sensitivity of the photon path length retrievals to subtle changes in atmospheric vertical structure.

5. Discussion and Conclusions

[24] We have developed an algorithm for retrieving two parameters of the photon path length probability density function (PDF) for both the oxygen A-band and the 0.820 μm water vapor band. We use solar direct-beam measurements to characterize the instrument response function in pixel (i.e., wavelength) space without the need to measure explicitly the solar spectral irradiance at the top of atmosphere, gaseous absorption coefficients, the instrument slit function or the pixel responses. Because the inverse Laplace transformation is by itself an ill-posed problem and the retrieval depends upon it, we constrain the inversion by assuming a gamma distribution for the photon path length PDF. Our choice of the gamma distribution was motivated by it being the actual photon path length PDF under optically thick cloud conditions. As illustrated by the χ-square contour analysis, the two-parameter gamma function constraint on the photon path length PDF is a reasonable assumption. We will explore algorithms with other constraints in an attempt to provide useful alternatives, particularly for studying stochastic models of radiative transfer [*Su and Pomraning*, 1994] and truncated Levy flight statistics [*Pfeilsticker*, 1999].

[25] As discussed in the paper by *Min et al.* [2001], knowledge of the mean photon path length allows some classification of cloud scenes, particularly identification of cases where cloud layering or complex structure is producing large photon path lengths and isolated subvisual cirrus is leading to reduced photon path lengths. With the development of the second-generation aRSS we are now able to retrieve the variance of the photon path length PDF in addition to its mean and for the 0.820 μm water vapor band as well as the oxygen A-band. As the two case study periods illustrate, the variance of the photon path length PDF is more sensitive than the mean photon path length to vertical cloud structure. Interestingly, the first two moments of the photon path length PDF exhibit sufficient sensitivity to detect cirrus that the millimeter-wave cloud radar may have failed to detect. Therefore photon path length information derived from passive measurements in the oxygen A-band and water vapor band in conjunction with radar and lidar measurements may provide a powerful remote sensing technique to characterize the geometric and optical properties of multilayer clouds. Additional study is warranted to investigate such a possibility by coupling ground-based oxygen A-band and cloud radar observations with satellite observations of clouds.

[26] Understanding changes in radiative heating associated with changes in vertical cloud and water vapor structures is crucial in studies of global climate change because atmospheric heating rates affect all aspects of the energy and hydrological cycles and are intimately involved in the feedbacks interrelating these cycles. Combining photon path length PDF information from both the oxygen A-band and 0.820 μm water vapor band provides us more insight into radiative transfer through various cloudy conditions, substantially improving our understanding of where water vapor absorbs solar radiation as both the water vapor and radiation is modulated by clouds. Joint statistics of the mean and variance of the photon path length PDF and cloud optical properties for both the oxygen A-band and the 0.820 μm water vapor band reveal the physical processes of radiation scattering and absorption in the atmosphere and may provide us further understanding of cloud-water vapor feedback. For multilayer cloud systems substantial photon path length enhancement may occur above the lowest layer cloud, while for single-layer cloud systems multiple scattering within the cloud plays a key role in enhancing photon path lengths. Therefore accurate knowledge of water vapor concentrations above low-level cloud and within all clouds is crucial to understanding heating rate profiles and the atmospheric energy balance.

[27] **Acknowledgments.** This research was supported by the National Science Foundation under grant ATM-9973701 and by the Office of Science (BER), U.S. Department of Energy, grants DE-FG02-03ER63531 and DE-FG02-90ER61071. Data were obtained from the Atmospheric Radiation Measurement (ARM) Program sponsored by the U.S. Department of Energy, Office of Energy Research, Office of Health and Environmental Research, Environmental Sciences Division.

References

Cahalan, R. F., W. Ridgeway, W. J. Wiscombe, T. L. Bell, and J. B. Snider, The albedo of fractal stratocumulus clouds, *J. Atmos. Sci.*, *51*, 2434, 1994.

Clothiaux, E. E., et al., Objective determination of cloud heights and radar reflectivities using a combination of active remote sensors at the ARM CART sites, *J. Appl. Meteorol.*, *39*, 645, 2000.

Fischer, J., and H. Grassl, Detection of cloud-top height from backscattered radiances within the oxygen A band, part 1: Theoretical study, *J. Appl. Meteorol.*, *30*, 1245, 1991.

Fischer, J., W. Cordes, A. Schmitz-Peiffer, W. Renger, and P. Morel, Detection of cloud-top height from backscattered radiances within the oxygen A band, part 2: Measurements, *J. Appl. Meteorol.*, *30*, 1260, 1991.

Grechko, Y. I., V. I. Dianov-Klokov, and I. P. Malkov, Aircraft measurements of photon paths in reflection and transmission of light by clouds in the 0.76 um oxygen band, *Atmos. Ocean Phys.*, *9*, 262, 1973.

Harrison, L., and Q.-L. Min, Photon pathlength distributions in cloudy atmospheres from ground-based high-resolution O_2 A-band spectroscopy, in *IRS'96: Current Problems in Atmospheric Radiation*, edited by W. L. Smith and K. Stamnes, p. 594, A. Deepak, Hampton, Va., 1997.

Harrison, L., M. Beauharnois, J. Berndt, P. Kierdron, J. Michalsky, and Q.-L. Min, The rotating shadowband spectroradiometer (RSS) at the Southern Great Plains (SGP), *Geophys. Res. Lett.*, *26*, 1715, 1999.

Heidinger, A., and G. L. Stephens, Molecular line absorption in a scattering atmosphere, 2: Retrieval of particle properties, *J. Atmos. Sci.*, *57*, 1615, 2000.

Intergovernmental Panel on Climate Change (IPCC), *Climate Change: The IPCC Scientific Assessment*, Cambridge Univ. Press, New York, 1990.

Intergovernmental Panel on Climate Change (IPCC), *Climate Change 2001: The Third Assessment Report*, Cambridge Univ. Press, New York, 2001.

Min, Q.-L., and L. C. Harrison, Cloud properties derived from surface MFRSR measurements and comparison with GOES results at the ARM SGP site, *Geophys. Res. Lett.*, *23*, 1641, 1996.

Min, Q.-L., and L. C. Harrison, Joint statistics of photon path length and cloud optical depth, *Geophys. Res. Lett.*, *26*, 1425, 1999.

Min, Q.-L., L. C. Harrison, and E. E. Clothiaux, Joint statistics of photon pathlength and cloud optical depth: Case studies, *J. Geophys. Res.*, *106*, 7375, 2001.

O'Brian, D. M., and R. M. Mitchell, Error estimates for retrieval of cloud top pressure using absorption in the A band of oxygen, *J. Appl. Meteorol.*, *31*, 1179, 1992.

Partain, P. T., A. K. Heidinger, and G. L. Stephens, High spectral resolution atmospheric radiative transfer application of the modified equivalence theorem, *J. Geophys. Res.*, *105*, 2163, 2000.

Pfeilsticker, K. F., First geometrical pathlengths probability density function derivation of the skylight from spectroscopically highly resolving oxygen A-band observations, 2: Derivation of the Levy index for the skylight transmitted by midlatitude clouds, *J. Geophys. Res.*, *104*, 4101, 1999.

Pfeilsticker, K., F. Erle, H. Veitel, and U. Platt, First geometrical pathlengths probability density function derivation of the skylight from spectroscopically highly resolving oxygen A-band observations, 1: Measurement technique, atmospheric observations and model calculations, *J. Geophys. Res.*, *103*, 11,483, 1998.

Portmann, R. W., S. Solomon, R. W. Sanders, and J. S. Danel, Cloud modulation of zenith sky oxygen path lengths over Voulder, Colorado: Measurements versus model, *J. Geophys. Res.*, *106*, 1139, 2001.

Stephens, G. L., Radiative effects of clouds and water vapor, in *Global Energy and Water Cycles*, edited by K. A. Browning and R. J. Gurney, pp. 71–90, Cambridge Univ. Press, New York, 1999.

Stephens, G. L., and A. Heidinger, Molecular line absorption in a scattering atmosphere, I: Theory, *J. Atmos. Sci.*, *57*, 1599, 2000.

Su, B., and G. C. Pomraning, A stochastic description of a broken cloud field, *J. Atmos. Sci.*, *51*, 1969, 1994.

Van de Hulst, H. C., *Multiple Light Scattering: Tables, Formulas, and Applications*, vol. 1, Academic, San Diego, Calif., 1980.

Veitel, H., O. Funk, C. Kruz, U. Platt, and K. Pfeilsticker, Geometrical path length probability density functions of the skylight transmitted by midlatitude cloudy skies: Some case studies, *Geophys. Res. Lett.*, *25*, 3355, 1998.

E. E. Clothiaux, Department of Meteorology, Pennsylvania State University, 603 Walker Building, University Park, PA 16802, USA. (cloth@essc.psu.edu)

Q. Min, Atmospheric Sciences Research Center, State University of New York, 251 Fuller Rd., Room L215, Albany, NY 12203, USA. (min@asrc.cestm.albany.edu)